SCIENTIFIC REPORTS

OPEN

SUBJECT AREAS:
TRANSPORTERS
DRUG DELIVERY

Received
27 September 2013

Accepted
7 January 2014

Published
25 February 2014

Correspondence and requests for materials should be addressed to Y.B. (yrbyun@snu.ac.kr)

Functional transformations of bile acid transporters induced by high-affinity macromolecules

Taslim A. Al-Hilal[1], Seung Woo Chung[1], Farzana Alam[2], Jooho Park[1], Kyung Eun Lee[3], Hyesung Jeon[3], Kwangmeyung Kim[3], Ick Chan Kwon[3], In-San Kim[3,4], Sang Yoon Kim[3,5] & Youngro Byun[1,2]

[1]College of Pharmacy, Seoul National University, Seoul 151-742, South Korea, [2]Department of Molecular Medicine and Biopharmaceutical Sciences, Graduate School of Convergence Science and Technology, College of Pharmacy, Seoul National University, Seoul 151-742, South Korea, [3]Center for Theragnosis, Biomedical Research Institute, Korea Institute of Science and Technology, Seoul 136-791, South Korea, [4]Department of Biochemistry and Cell Biology, School of Medicine, Kyungpook National University, Daegu 700-422, South Korea, [5]Department of Otolaryngology, Asan Medical Center, College of Medicine, University of Ulsan, Seoul 138-736, South Korea.

Apical sodium-dependent bile acid transporters (ASBT) are the intestinal transporters that form intermediate complexes with substrates and its conformational change drives the movement of substrates across the cell membrane. However, membrane-based intestinal transporters are confined to the transport of only small molecular substrates. Here, we propose a new strategy that uses high-affinity binding macromolecular substrates to functionally transform the membrane transporters so that they behave like receptors, ultimately allowing the apical-basal transport of bound macromolecules. Bile acid based macromolecular substrates were synthesized and allowed to interact with ASBT. ASBT/macromolecular substrate complexes were rapidly internalized in vesicles, localized in early endosomes, dissociated and escaped the vesicular transport while binding of cytoplasmic ileal bile acid binding proteins cause exocytosis of macromolecules and prevented entry into lysosomes. This newly found transformation process of ASBT suggests a new transport mechanism that could aid in further utilization of ASBT to mediate oral macromolecular drug delivery.

ASBT is a membrane transporter that moves endogenous small molecular bile acid conjugates for the maintenance of enterohepatic bile acid circulation from the apical surface of enterocytes and cholangiocytes to the cytoplasm[1–3]. In the transport of bile acids, several transmembrane domains (TD) of ASBT are coordinated to create a hydrophobic substrate-binding pocket. The binding of substrates in this extracellular pocket, along with sodium binding, drives the conformational change between the outward- and inward-facing states of ASBT, which in-turn, opens the cytoplasmic channel of ASBT to traverse bile acids[4]. Bile acids are then bound to ileal bile acid-binding protein (IBABP), shuttled across the cytoplasm to the basolateral membrane, and finally exported into the blood circulation by basolateral transporters such as organic solute transporter (OST-α/β)[5–8]. Because of this intriguing involvement of membrane transporters, the physiology of the bile acid transport system has received considerable attention in the quest to shuttle small molecular pharmaceutical drugs. However, the challenge lies with respect to macromolecular transport because the membrane-based transporters follow the non-vesicular transport mechanism that allows intercompartmental transfer of only small molecules by means of facilitated transport[9,10].

Membrane-based receptors follow the endocytosis process, by which extracellular molecules bound to their cognate receptors on the cell surface can ferry cargos between subcellular organelles, irrespective of the cargo size[11,12]. Once endocytosed, the receptors are trafficked through and fused with acidic organelles, such as lysosomes, where acid-dependent hydrolases facilitate the dissociation of the cargo from the receptor[13]. Utilization of receptors such as vitamin-B_{12} receptors and Fc receptors[13–15] appears to be a practical strategy for macromolecular drug delivery. However, it poses a high risk of failure because these receptors are either inadequately distributed or heterogenically expressed in the intestine, and in most cases macromolecular drugs are degraded by lysosomal enzymes. On the other hand, apical transporters such as ASBT, peptide transporters, or OATP transporters, are desirable for the delivery of orally administered macromolecules since they are highly expressed in the intestine and are not susceptible to lysosomal degradation in the transport process[16,17]. Unfortunately, transporters do not

internalize like the receptors to transport their substrates across the cell, because of which the uptake is size-limited.

Here, we describe a novel mechanism of delivering macromolecules via ASBTs by inducing vesicular transport, which has not been previously observed. In our previous study, deoxycolic acid (DOCA)-based oligomeric substrates (*oligo*DOCA) for ASBT, namely dimeric, trimeric, and tetrameric deoxycholic acids (*bis*DOCA, *tri*DOCA, *tetra*DOCA, respectively), were synthesized and conjugated to a model macromolecule, low molecular weight heparin (LMWH; Supplementary Fig. S1 online). On the basis of previous studies, we demonstrated that a unique oligomeric bile acid analogue, *tetra*DOCA, could enhance the absorption of macromolecular LMWH in the GI tract by site-specific conjugation without compromising the bioactivity of LMWH itself. LMWH-*tetra*DOCA conjugate (LHe-*tetra*D) showed a specific binding to ASBT; however, the underlying absorption mechanism was not known. In this study, we found that LHe-*tetra*D, being a high-affinity substrate, induced functional transformation of ASBT. This allowed the apical-to-basal transport of ASBT/LHe-*tetra*D complexes in vesicles. In the cytoplasm, ASBT/LHe-*tetra*D complexes were dissociated from each other via interaction of LHe-*tetra*D with IBABP. This eventually led to the exocytosis of LHe-*tetra*D and prevented its entry into the lysosomal compartment. ASBT also recycled back to the membrane, as a consequence. Thus, the functional transformation of ASBT to induce vesicular transport enabled the transport of macromolecular LHe-*tetra*D.

Results

Binding affinity between LHe-*tetra*D and ASBT. The structure of *tetra*DOCA and its LMWH conjugate is shown in Supplementary Figure S1 online. Binding affinities, which are reflected by the dissociation rate constants at equilibrium (K_D) between the mono or *oligo*DOCA derivatives and rhASBT, have been examined previously. In that study, the K_D of *mono*DOCA with ASBT remained weak to moderate (0.189 μM); however, *tetra*DOCA exhibited a significantly lower K_D (0.003 μM) toward the ASBT. Considering the high binding affinity of *tetra*DOCA with ASBT, we designed an LMWH analogue having *tetra*DOCA moiety. In this study, the binding of LHe-*tetra*D to ASBT was also investigated by using surface plasmon resonance. LHe-*tetra*D showed high affinity to ASBT with a low dissociation rate constant of $K_D = 0.072$ μM (Fig. 1a).

Distribution of ASBT in the presence of LHe-*tetra*D in cells. ASBT-transfected MDCK cells were treated with sodium taurocholate (TCA; 200 mM), a small molecular weight substrate, and 0.05 mg/mL of LHe-*tetra*D. The distribution of ASBT from membrane to cytoplasm was checked by western blot analysis and confocal microscopy. Membrane, cytoplasmic, and nuclear fractions were collected following drug treatment. Surprisingly, ASBT was spatially shifted from the membrane to the cytoplasm, but not to the nucleus, in LHe-*tetra*D-treated ASBT-transfected MDCK (MDCK-ASBT) cells (Fig. 1b). In contrast, TCA did not induce any such translocation of ASBT. The removal of LHe-*tetra*D caused retro-translocation of ASBT from the cytoplasm to the membrane. In confocal images obtained from LHe-*tetra*D-treated Caco-2 and MDCK-ASBT cells, intracellular ABST fluorescence intensity was markedly increased within the cells as compared to the control cells (Fig. 1c, d). These results suggest that LHe-*tetra*D induces translocation of ASBT from the membrane to the cytoplasm.

ASBT mediated macromolecular LHe-*tetra*D transport. Since the transport capacity of ASBT in controlled by regulated insertion of ASBT into the plasma membrane and dephosphorylation at serine and threonine sites[18,19], we first evaluated the effect of LHe-*tetra*D on the phosphorylation of ASBT. We did not observe any changes in the tyrosine phosphorylation of ASBT in LHe-*tetra*D treated MDCK-ASBT cells, compared to the control (Fig. 2a). To determine whether the ASBT translocation indeed caused the transport of macromolecular LHe-*tetra*D, we performed co-immunoprecipitation assays in MDCK-ASBT cells. Complexes of ASBT and LHe-*tetra*D were isolated from membrane fractions as well as from cytoplasmic fractions of the treated cells (Fig. 2b). The extensive co-localization of ASBT and LHe-*tetra*D was also visualized by immunofluorescence studies (Fig. 2c).

To further confirm the relationship between ASBT translocation and LHe-*tetra*D transport, an *in situ* proximity ligation assay (PLA) was employed. ASBT/LHe-*tetra*D complexes (red dots) were formed *in situ*, which were distributed in the membrane and internalized rapidly into the early endosomes en route to the cytoplasm (Fig. 3a, b). Co-localization between red dots and the early endosomal marker, EEA-1, was confirmed by Pearson coefficients greater than 0.5 (Fig. 3b). These results suggest that ASBT first forms complexes with LHe-*tetra*D at the apical membrane where it is primarily localized, and then facilitates the transcellular entry of LHe-*tetra*D into the cytoplasm.

Formation of vesicles containing ASBT/LHe-*tetra*D. ASBT, but not LHe-*tetra*D, was found to interact in abundance with phosphatidic acid (PA) and phosphatidylserine (PS) rather than with a subset of inositol head-group phospholipids and sphingolipids (Supplementary Fig. S3 online). ASBT might be anchored to PA, which has a direct influence on the membrane bending or destabilization owing to its physical properties[20]. When the concentration of the binding substrate or protein exceeds the dissociation rate constant, any protein-protein interactions with high affinity would have the greatest tendency to facilitate membrane curvature and consequent internalization[21]. TEM analysis revealed a larger number of vesicles in the cytoplasm of both LHe-*tetra*D-treated MDCK-ASBT and Caco-2 cells (Supplementary Fig. S4 online).

The TEM results from immunolabelling with ASBT antibody-labeled gold nanoparticles revealed an internalization process by the vesicle formation (Fig. 4a–f). Gold-marks representing ASBT (arrow) were primarily detected in the membrane of MDCK-ASBT cells (Fig. 4a). LHe-*tetra*D caused the cell membrane to morphologically change into a concave curvature by binding with ASBT, which then formed vesicles (Fig. 4b, c). The vesicles containing ASBT were fused with the adjacent vesicles, thereby forming multi-vesicular bodies (MVB) in the cytoplasm (Fig. 4d, e). Therefore, the dynamic functional transformation of ASBT by vesicular transport represents a key step to foresee an expanded model for the uptake of LHe-*tetra*D.

Interaction of LHe-*tetra*D with IBABP and membrane recycling of ASBT. It is well established that IBABP specifically interacts with bile acids in the cytoplasm and shuttles them to the basolateral membrane, where bile acids are finally exocytosed to the blood circulation. When LHe-*tetra*D was treated to SK-BR-3 cells, which naturally express both ASBT and IBABP, co-localization of LHe-*tetra*D with ASBT in the vesicle was confirmed (Supplementary Fig. S5 online). Using biotin pull-down assay, we assessed whether LHe-*tetra*D and IBABP interacted with each other. Complexes of LHe-*tetra*D-biotin and IBABP were isolated from the whole-cell lysate of treated SK-BR-3 cells (Fig. 5a). LHe-*tetra*D-biotin was also observed to interact with ASBT at the same time. The intracellular co-localization of LHe-*tetra*D and IBABP was also visualized (Fig. 5b). Using PLA, we found that LHe-*tetra*D could form a complex with IBABP and finally dissociated from ASBT (Fig. 5c). Dissociated ASBTs entered the Rab11-positive recycling endosomes (Fig. 5srd and Supplementary Fig. S6 online). Notably, LHe-*tetra*D was not co-localized with LAMP-1-positive lysosomes (Supplementary Fig. S7 online). Therefore, these results indicate that IBABP binds with LHe-*tetra*D in the cytoplasm, and then the bound

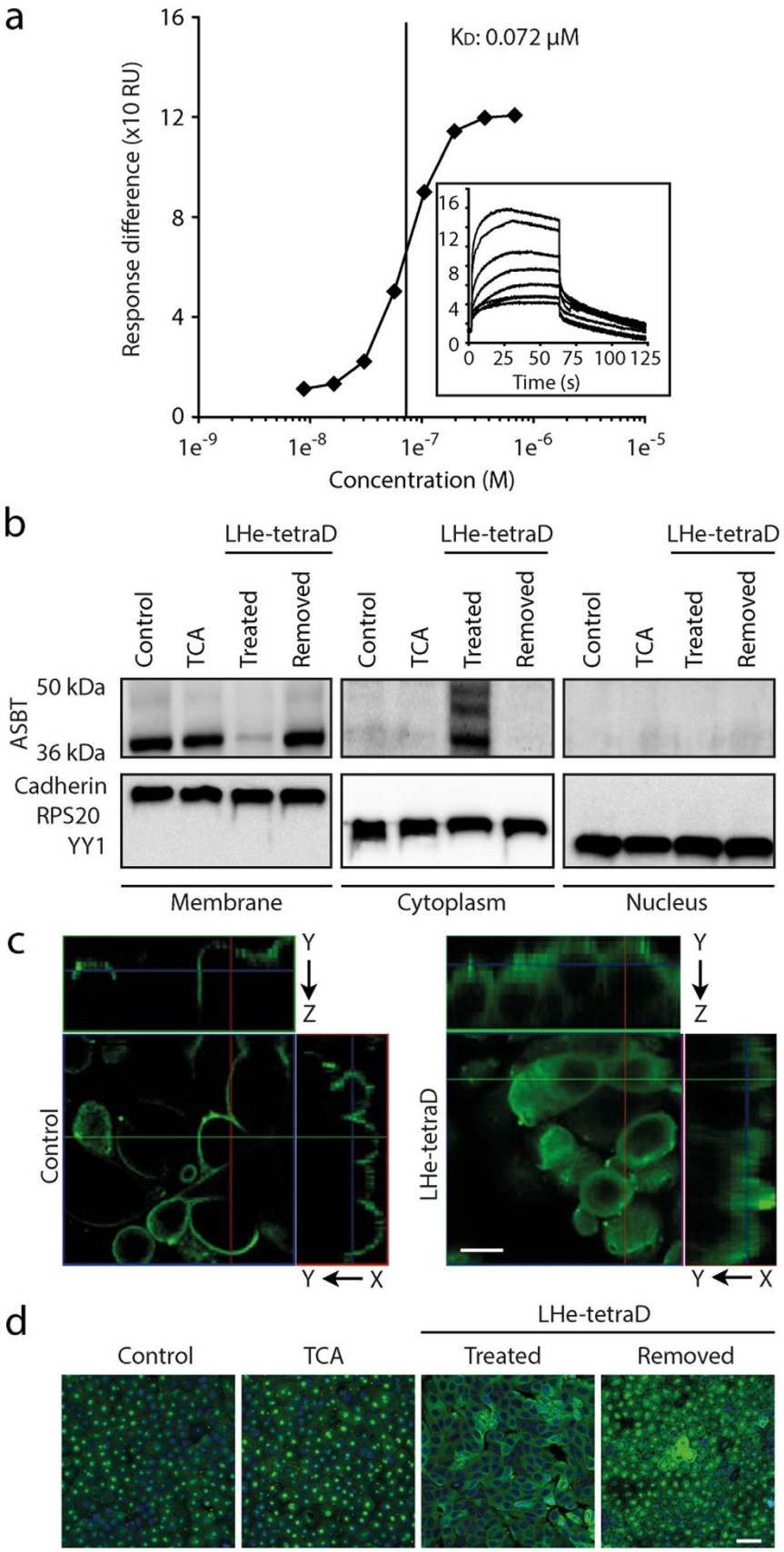

Figure 1 | Distribution of ASBT due to the treatment of high-affinity binding LHe-*tetra*D in cells. (a) Binding affinity of tetrameric deoxycholic acid (*tetra*DOCA) conjugated LMWH derivative (LHe-*tetra*D) with ASBT. The dose-response curve of LHe-*tetra*D binding to immobilized human ASBT protein. (b) Changes in the ASBT membrane expression after LHe-tetraD and sodium taurocholate (TCA) treatment in the MDCK-ASBT cells. To facilitate representation, the blots are cropped and the full-length blots are presented in the supplementary Figure S7. The translocation of ASBT (green) from membrane to cytoplasm was observed in both (c) Caco-2 cells; scale bar, 10 μm, and (d) MDCK-ASBT cells; scale bar, 20 μm.

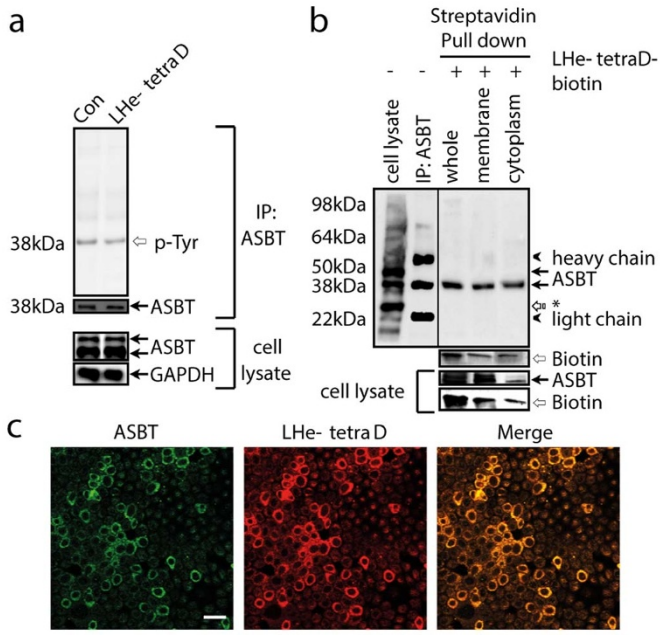

Figure 2 | Physical interactions of ASBT and LHe-*tetra*D in cells. (a) Immunoprecipitation-immunoblot analysis for p-ASBT (IP-ASBT, IB-pTyr) and the total ASBT (IP-ASBT, IB-ASBT) from the non-treated and LHe-*tetra*D-treated MDCK-ASBT cells. (b) Biotin-labeled LHe-*tetra*D was incubated with MDCK-ASBT cells and pulled-down by streptavidin beads from membrane and cytoplasmic fraction as well as from the whole cell lysates, followed by immunoblotting for bound ASBT protein and biotin. The control included the ASBT band from lysates and the immunoprecipitates of the non-treated MDCK-ASBT cells. Asterisk indicates non-specific band; (c) The co-localization of LHe-*tetra*D (red) and ASBT (green) were also visualized in MDCK-ASBT cells. Scale bar indicates 20 μm.

LHe-*tetra*D subsequently dissociates from the vesicles. However, it is not clear how LHe-*tetra*D can escape from the vesicle to bind with IBABP.

Distribution of ASBT in the presence of LHe-*tetra*D in rat intestine. The induced functional transformation process of ASBT by LHe-*tetra*D observed *in vitro* was reaffirmed *in vivo* in the ileum of treated rats. At first, coumarin-labeled LHe-*tetra*D was administered orally to rats, which confirmed the small intestine as the main absorption site (Supplementary Fig. S8a online). The ileum had 2–4 times higher fluorescent intensity per unit area at 0.5 and 2 h than the duodenum and 5–15 times higher fluorescence than the jejunum at 4 h. To confirm the absorption mechanism *in vivo*, RITC-labeled LHe-*tetra*D was orally administered to rats and different segments of small intestine were isolated 1 h later. The segments were fixed, treated with phalloidin-FITC (actin marker) and DAPI (to stain the nucleus), and imaged using confocal microscope. LHe-*tetra*D was detected in the lamina propria of small intestine, indicating its trans-epithelial absorption (Supplementary Fig. S8b online). After LHe-*tetra*D treatment, the ASBT intensity gradually shifted from the apical mucosa to the sub-apical mucosa, which reversed with time, as revealed by immunohistochemistry (IHC) analysis (Fig. 6a). However, the total ASBT expression in the rat ileum remained unchanged (Fig. 6b). Interestingly, the intensity and expression of IBABP was increased at the sub-apical mucosa, as shown by IHC and western blot analysis, respectively (Fig. 6c, d). The expression of IBABP was also diminished gradually with time. The results comprehensively elucidate the significance of ASBT internalization in response to LHe-*tetra*D *in vivo*, and the role of IBABP in transporting LHe-*tetra*D from the cytoplasm to the basolateral membrane throughout the small intestine.

On the basis of our findings, we propose here a new transport mechanism in the place of the conventional ASBT transport mechanism (Fig. 7). In the conventional mechanism, ASBT transports small molecule bile acids solely through its membrane-spanning domains. In the newly proposed mechanism, ASBT is internalized and functions like a receptor to circumvent the size limitation in its transport system.

Discussion

Transporters facilitate the membrane permeation of its substrates against the concentration gradient, which is energetically driven. Thus, bile acid transporters utilize the sodium ion dependent unidirectional transport mechanism to drive the substrates (small molecule bile acids) across the cell, a feature that is impedimental to transporting macromolecules like bile acid conjugates. Here, we describe the development of high-affinity binding oligomeric bile acid conjugate, LHe-*tetra*D, which causes functional transformation of ASBT upon interaction. This internalization process allows ASBT to transport the bound LHe-*tetra*D to the other side of the membrane. Based on the results of our *in vitro* and *in vivo* studies, we argue that ASBT, bound at the apical membrane through its association with the spanning TDs with phospholipids, which are mostly phosphatidic acid and phosphatidylserine, is dissociated when it comes in contact with LHe-*tetra*D. An intimate contact between ASBT and LHe-*tetra*D allows the accumulation of ASBT at the curved regions of cells that literally leads to membrane budding. Such membrane budding by molecular crowding has also been proposed recently not only for membrane curvature associated receptors but also for any membrane-bound proteins, such as membrane-bound GFP[22,23]. Lateral pressure generated by the interaction between ASBT and LHe-*tetra*D may aid this membrane budding formation by lowering the bending energy and partitioning to its negative curvature region, thereby enabling cytoplasmic translocation. This translocation of ASBT is in agreement with LHe-*tetra*D translocation, both of which are enabled through vesicle formation and internalized rapidly into EEA-1-positive early endosomes. Early endosomes containing ASBT/LHe-*tetra*D complexes are eventually fused with existing vesicles to form MVBs in the cytoplasm, where the ASBT/LHe-*tetra*D complexes might dissociate from each other and escape the vesicular transport. To explain the mechanism by which LHe-*tetra*D escapes from the endosomes, the following hypotheses may be envisioned; 1) The lowered pH of theses organelles in polarized epithelial cell lines usually causes the dissociation of receptors from their ligands[24–27]. It is hence hypothesized that the decreased luminal pH of endosomes might also provide the environment in which LHe-*tetra*D can be dissociated from the ASBT. 2) The protonation of carboxylic moieties of LHe-*tetra*D due to the lowered pH in the endosomes can increase hydrophobicity of LHe-*tetra*D, thereby enhancing its permeability through the endosomal membrane. 3) Due to the buffering capacity of LHe-*tetra*D, more protons and ions might be pumped into the endosomes, which could induce an influx of water[28,29]. Eventually, the osmotic pressure might cause the endosomal membrane to become permeable enough for the soluble macromolecules to pass through. Based on the combined effect of the above factors, LHe-*tetra*D can be released into the cytoplasm from the endosomes. Further studies will be conducted to study the detailed mechanism. The dissociation of ASBT/LHe-*tetra*D complexes eventually promotes the retro-translocation of ASBT back to the membrane via Rab11-positive recycling endosomes. The dissociated LHe-*tetra*D is then transported to the basolateral part as a complex with cytoplasmic IBABP and is consequently removed by exocytosis without entering the LAMP-1 positive lysosomal compartment.

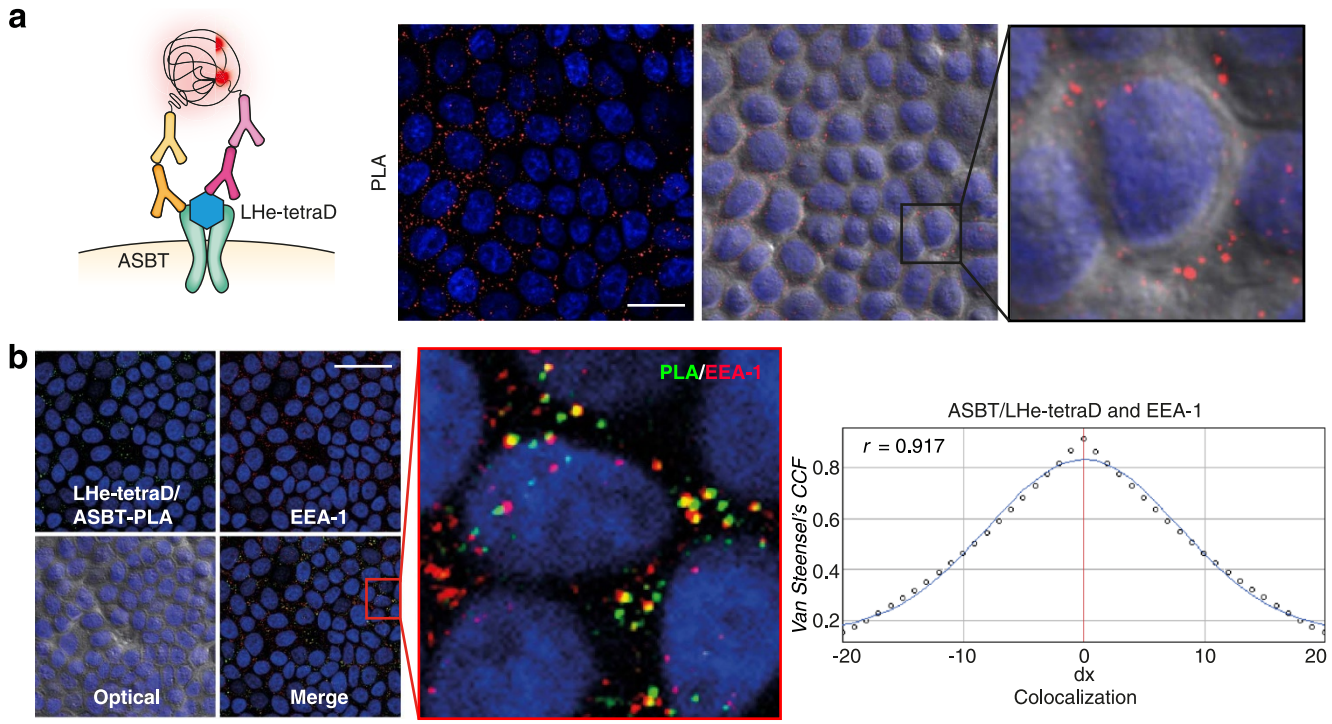

Figure 3 | Visualization of ASBT and LHe-*tetra*D complex internalization in cells. (a) Proximity ligation assay (PLA; red dot) between ASBT and biotin-labeled LHe-*tetra*D in MDCK-ASBT treated cells. Scale bar indicates 20 μm. (b) The co-localization of PLA-labeled ASBT/LHe-*tetra*D complexes (green) with early endosome marker EEA-1 (red) in MDCK-ASBT cells. Scale bar indicates 20 μm. The co-localization analysis performed on original images using Van Steensel's cross-correlation coefficient (CCF) between PLA labeled ASBT/LHe-*tetra*D and EEA-1 with JACop software. The perfect bell-shaped curves and Pearson coefficient (*r*) ranging from 0.8 to 1 were observed for the ASBT/LHe-*tetra*D complexes with EEA-1 (right panel).

We demonstrated that in the ASBT expressing intestinal epithelial cells and rat ileum, a deoxycholic acid-based tetramer conjugated LMWH induced internalization of ASBT. We also demonstrated that, due to the intracellular involvement of IBABP in the transport process, neither ASBT nor LHe-*tetra*D entered into the lysosomal compartments, where macromolecular drugs are likely to be degraded by hydrolytic enzymes. LHe-*tetra*D also induced the redistribution of ASBT *in vivo*, as shown by IHC analysis. Consistent with these findings, we previously found that LHe-*tetra*D was absorbed orally and effectively induced anticoagulation to successfully inhibit systemic thrombus formation. Thus, the new transport mechanism of ASBT described here is of major importance for patients and physicians, because it might lead to ASBT-mediated macromolecular drug delivery. However, further studies will be required to find out whether the proposed vesicular transport mechanism of ASBT via receptor-like functional transformation would also work for the oral delivery of other macromolecular drugs such as, proteins, polypeptides etc. Furthermore, these

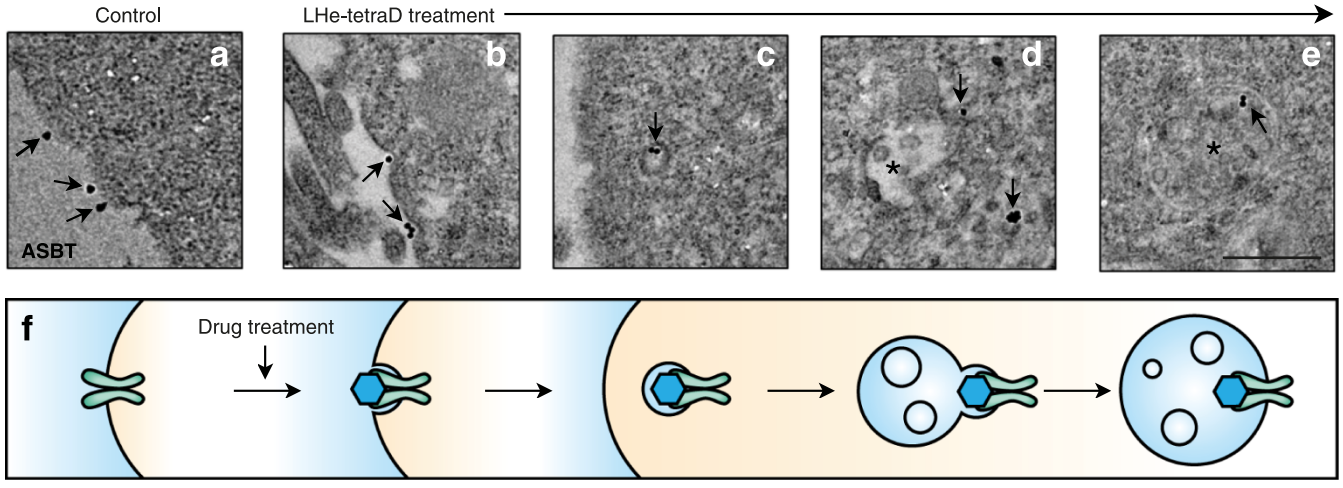

Figure 4 | LHe-*tetra*D stimulates ASBT internalization in vesicles. The vesicular transport of ASBT (a–e) as illustrated by the schematic representation (f) was observed by TEM. ASBT was detected (arrow) in the membrane of MDCK-ASBT cells as gold-marks (a). Following the LHe-*tetra*D treatment, the gold-marks appeared in distinctively concave-shaped membrane curvatures (b), in vesicles near the membrane (c), and in the multi-vesicular bodies (asterisks) in the cytoplasm (d and e). Scale bar indicates 200 nm.

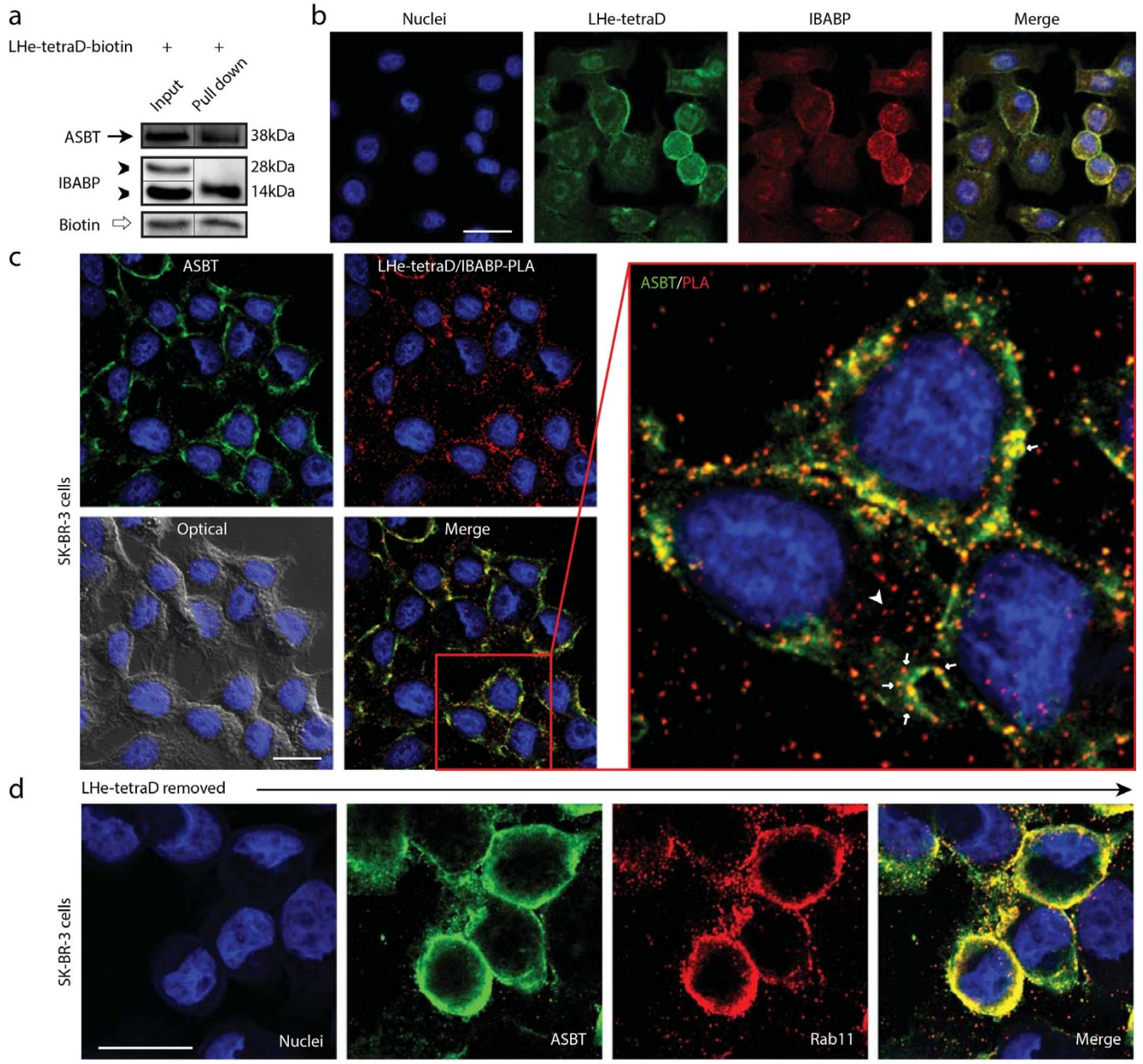

Figure 5 | Interaction of LHe-*tetra*D with IBABP and retro-translocation process of ASBT. (a) The interaction between LHe-*tetra*D and IBABP along with ASBT in SK-BR-3 cells. To facilitate representation, the blots are cropped and the full-length blots are presented in the Supplementary Figure S7. (b) The colocalization of individually labeled LHe-*tetra*D (green) and IBABP (red) in SK-BR-3 cells (nucleus, blue). Scale bar indicates 10 μm. (c) PLA between IBABP and the biotin-labeled LHe-*tetra*D in the SK-BR-3-treated cells. Scale bar indicates 10 μm ASBT is stained as green. Arrowheads indicate the co-localization of LHe-*tetra*D/IBABP-PLA and ASBT in the membrane. Arrow indicates that the complexes of LHe-*tetra*D/IBABP (red dots) are being dissociated from ASBT in the cytoplasm. (d) SK-BR-3 cells were treated with LHe-*tetra*D for 30 min, washed and incubated for additional 15 min at 37°C in HBSS before staining. The extensive co-localization of individually labeled ASBT (green) and Rab11 (red), a marker of recycling endosome, indicated that free ASBTs were located in the recycling endosomes for membrane retro-translocation. Scale bar indicates 10 μm.

findings might shed light on the underpinning of the functional transformation process of membrane transporters and the synthesis of specific, high-affinity binding substrates.

Methods

Materials. Deoxycholic acid (DOCA)-based ASBT substrates were synthesized as described in the previous study, namely monomeric, dimeric, trimeric, and tetrameric deoxycholic acids (monoDOCA, bisDOCA, triDOCA, tetraDOCA, respectively) and the substrates were further conjugated with LMWH to synthesize the conjugates, namely LHe-monoD, LHe-bisD, LHe-triD, and LHe-tetraD, respectively. The Institutional Committee of Seoul National University approved all the reagents, experimental protocols, and animal experiments.

Binding affinity study with human ASBT. Binding measurement between LHe-*tetra*D and recombinant human ASBT (rhASBT) was performed by surface plasmon resonance on a BIAcore T100 (GE Healthcare, Uppsala, Sweden). The sample analyte, LHe-*tetra*D, was prepared at concentrations ranging from 2 to 0.0078 μM in 0.5% DMSO containing HEPES buffer supplemented with 150 mM NaCl, which was also used as a running buffer. To immobilize rhASBT, the surface of a CM5 sensor chip (GE Healthcare, Uppsala, Sweden) was activated using the amide-coupling method. The immobilization of rhASBT was controlled to achieve 400–500 response units. The flow rate of analyte was adjusted to 20 μL/min. To regenerate the surface of the sensor chip, 50 mM NaOH was discharged after each cycle of analysis. Each concentration was run in triplicate. The data were analyzed for curve fitting using BIAcore T100 evaluation software (GE Healthcare).

Evaluation of ASBT distribution in cells. To monitor the spatial distribution of ASBT by using the LHe-*tetra*D treatment, the distribution of ASBT was evaluated

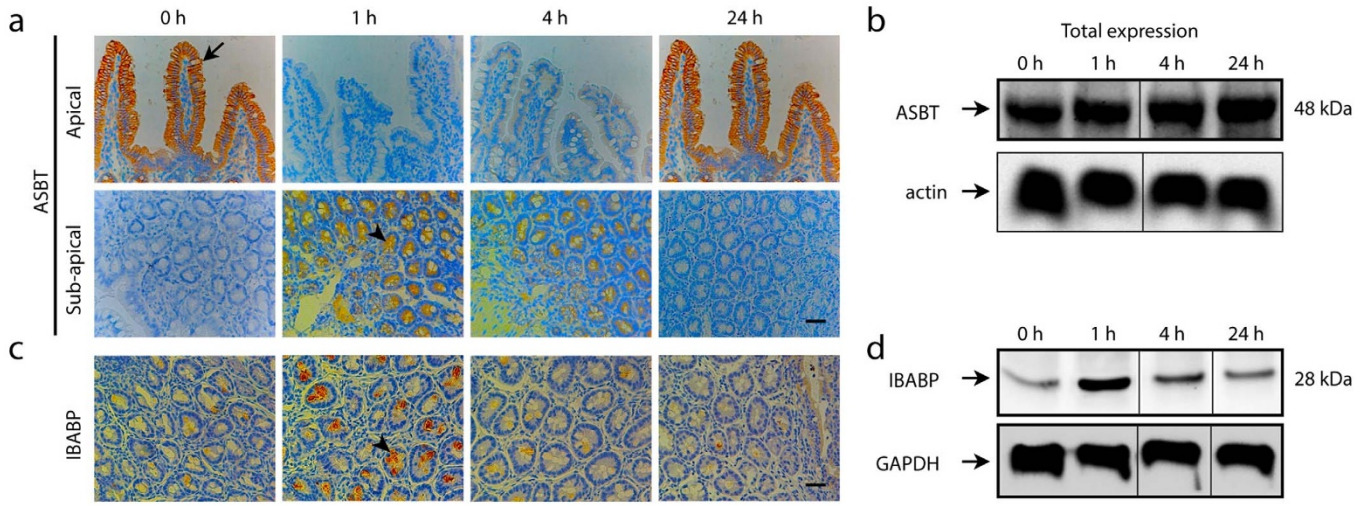

Figure 6 | Redistribution of ASBT *in vivo* after LHe-*tetra*D treatment. (a) The internalization of ASBT from the apical membrane (arrow) to the sub-apical mucosa (arrowhead) of rat ileum following treatment with LHe-*tetra*D. At 24 h after LHe-*tetra*D administration, ASBT were recycled back to the apical region as that of the control group. (b) Note that the total ileum ASBT protein expression was not changed. IBABP staining and expression in the sub-apical mucosa (arrowhead) of rat ileum following treatment with LHe-*tetra*D as shown by immunohistochemistry (c) and western blot analysis (d) from the whole-tissue lysates. Scale bars indicate 50 μm. To make a better representation, the blots are cropped and the full-length blots are presented in the supplementary Figure S7.

from the fractions of MDCK-ASBT cells by immunoblotting. Membrane and cytoplasmic fractions were collected using the FractionPREP™ cell fractionation kit (Biovision, CA) by following the procedure described in the protocol with slight modifications. Briefly, 100% confluent MDCK-ASBT cells were pre-incubated with a metabolic inhibitor buffer and treated with the samples for 5 min. The cells, in another LHe-*tetra*D-treated group, were washed and incubated for an additional 15 min at 37°C in HBSS. The cells were then harvested in ice-cold PBS, and centrifuged. The cell sediment was resuspended in 300 μL of cytosol extraction buffer-mix (containing DTT and protease inhibitor cocktail). The samples were incubated on ice for 20 min with gentle tapping every 5 min and centrifuged at 700 × *g* for 10 min. The supernatant was collected as cytoplasmic fraction. After each fractionation, the pellets were washed once with HBSS and centrifuged. The remaining pellet was resuspended in 300 μL of membrane extraction buffer-A mix (containing DTT and protease inhibitor cocktail). The mixture was vortexed, followed by the addition of 20 μL of membrane extraction buffer-B. The suspended pellets were placed on ice for 1 min, vortexed twice and centrifuged at 3400 rpm for 5 min. The supernatant was collected as membrane fraction. Nuclear fractions were collected using the following method. The cells were treated, washed, collected in ice-cold PBS, and centrifuged as previously described. The cell sediment was resuspended in a hypotonic buffer [10 mM HEPES (pH 7.9), 10 mM KCl, 1.5 mM $MgCl_2$, 12 mM β-glycerophosphate, 10 mM NaF, 1 mM Na_3VO_4, PMSF, protease inhibitor, EGTA], placed on ice for 10 min, vortexed gently, and centrifuged at 1500 rpm for 3 min. The supernatant was collected and stored. This procedure, with the exception of the 5-min incubation, was repeated and the collected supernatant was discarded. The remaining pellet was resuspended in another hypotonic buffer [20 mM HEPES-KOH (pH 7.9), 420 mM NaCl, 1.5 mM $MgCl_2$, 0.2 mM EDTA, EGTA, 20% glycerol supplemented with 1 mM DTT, 20 mM β-glycerophosphate, NaF, PMSF, protease inhibitor, phosphatase inhibitor], vortexed, and incubated for 30 min. The mixture was vortexed at 5-min intervals, and finally centrifuged at 14,000 rpm for 10 min. The supernatant was collected as nuclear extract and preserved in −80°C until analyzed.

Protein concentration was determined using a BCA protein assay kit (Pierce Biotechnology, Rockford, IL). The purity of each fraction was confirmed by western blotting using a specific marker. Antibodies against Pancadherin, RPS20, and YY1 (H-10), were used as markers for the membrane, cytoplasm, and nuclear cell fractions, respectively (Supplementary Fig. S2 online). The negative staining of membrane marker in the cytoplasmic fraction or cytoplasmic marker in the membrane or nuclear fraction was taken as a confirmation of the purity of each fraction. A total of 50 μg of protein was loaded in a 12% Tris-glycine gradient gel (Bio-Rad Laboratories, CA) for the sodium dodecylsulfate-polyacrylamide gel electrophoresis (SDS-PAGE) analysis. The membranes were probed with ASBT (C-terminal) antibodies followed by the incubation with the HRP-conjugated secondary antibody.

Immunofluorescence (IF) studies. For IF staining, the cells were fixed with 200 μL of 4% cold paraformaldehyde (PFA) solution in PBS for 20 min at room temperature, followed by permeabilization in 0.3% Triton X-100 in a blocking solution prepared from 10% normal goat serum in PBS for 40 min. Biotin and ASBT antibodies were used to detect LHe-*tetra*D-biotin and ASBT, respectively, at a dilution of 1 : 100 in the diluted blocking buffer overnight. The primary antibodies were stained with Alexa Flour®488 (green) and Alexa Flour®555 (red)-labeled secondary antibodies. Nuclei were counterstained with Hoechst 33258 dye. Fluorescence images were then observed under a confocal microscope (Carl Zeiss LSM710, Leica DM IRB/E; Leica Co., Germany).

Caco-2 cell or MDCK-ASBT cell monolayers were incubated with EEA-1, Rab11, or LAMP-1 antibodies. The primary antibodies were then counter stained with Alexa Flour®555 (red)- and Alexa Flour®488 (green)-labeled secondary antibodies. Co-localization was analyzed using JACop software. Co-localization between molecules was indicated by a Pearson coefficient (*r*) ranging from 0.8 to 1, and a bell-shaped curve with a peak at $\delta x = 0$ by the Van Steensel's cross-correlation coefficient (CCF)[30,31].

Transmission electron microscopy (TEM) analysis using immunolabeled gold particles. Both Caco-2 and MDCK-ASBT cells were treated with LHe-*tetra*D at 37°C for 5 min, fixed with 2.5% glutaraldehyde, dissolved in 0.1 M cacodylate buffer overnight at 4°C, and then in 2% osmium-tetroxide for 1 h. The cells were dehydrated with an ethanol series, infiltrated with Spurr's resin series, and polymerized at 60°C for 8 h. The embedded cells were cut with a diamond knife on an ultramicrotome (MTX-L, RMC). The sections were mounted directly on 150-mesh nickel grids. At this point, the grids were examined using a transmission electron microscope to compare the formation of vesicles with respect to non-treated cells. For gold labeling, the sections were further treated with 0.1 M citrate buffer and then 3% H_2O_2. The sections were then blocked using AURION blocking reagent for 30 min and incubated overnight with anti-ASBT (N-terminal). The sections were then rinsed with 0.1% BSA-C (AURION) in PBS and incubated with the 20-nm gold-conjugated anti-rabbit antibody for 1 h. After washing with 0.1% BSA-C in PBS, the sections were treated with 0.2% glutaraldehyde and washed with distilled water. The sections were stained with 2% uranyl acetate solution for 10 min and with Reynold's lead citrate solution for 5 min. The grids were examined using a Tecnai F20 electron microscope (FEI Electron Microscopes, Hillsboro, OR) at 200 KV.

Animal experiments. All the animal experiments were carried out according to the regulations of the Institutional Animal Ethics Committee of Seoul National University animal care facility, as described in the Regulation for the Care of Animals (29/02/2008, No. 8852). To evaluate intestinal absorption of LHe-*tetra*D, RITC-labeled LHe-*tetra*D was orally administered to male SPF, Sprague-Dawley rats (weighing approximately 250 g, Korean Animal Center, Korea) that had been fasting for 8 h. One h after oral administration of LHe-*tetra*D-RITC, the rats were sacrificed and 2.5-cm segments of the small intestine were removed, and prepared for histological analysis. Actin filaments and nuclei were stained with phalloidin-FITC and DAPI, respectively. To evaluate the site of drug absorption, coumarin was tagged to LHe-*tetra*D as a green fluorescent marker, and administered as mentioned above with sampling time points at 0.5, 1, 2, and 4 h. Fluorescent coumarin was extracted from the tissues by incubation in formamide for 48 h at 25°C. Samples were centrifuged, and the intensity of fluorescent signals from supernatants was detected using a Wallac 1420 VICTOR plate-reader (Perkin-Elmer Life Sciences, MA) with excitation/emission at 488 nm/530 nm. Tissue auto-fluorescence was corrected by subtracting the fluorescent signal of non-treated rat tissues from fluorescent signal in the treated rats.

The ileums from untreated and treated rats before and at 1, 2, 4, and 24 h after drug administration were excised and embedded immediately in OCT. Ten to 12 sections

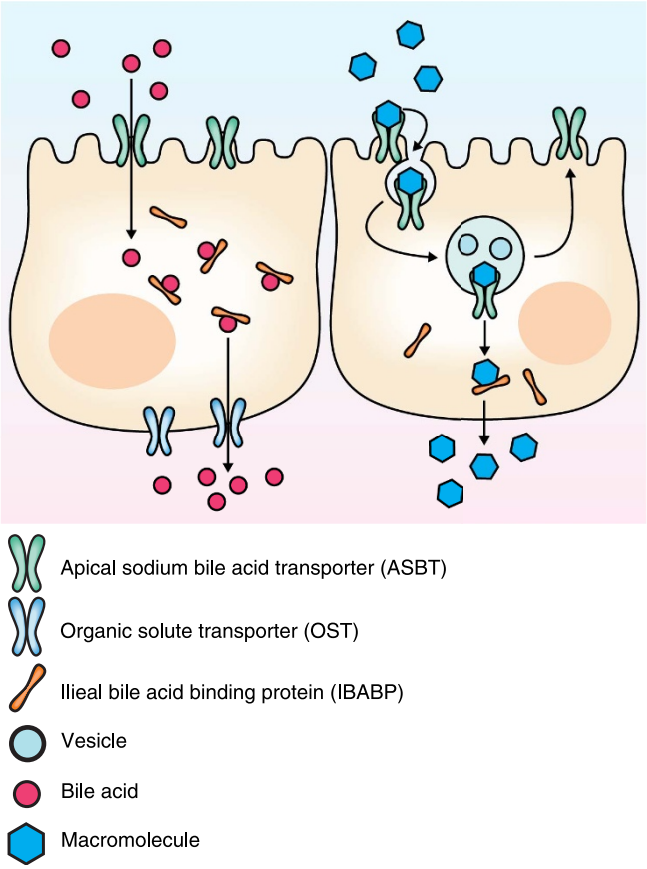

Figure 7 | The schematic of the new model for the ASBT transport mechanism. In the conventional transport mechanism, ASBT moves only small molecule substrates into the cytoplasm through its transmembrane domain. In the newly proposed vesicular transport mechanism, the transformation of ASBT can be induced by high-affinity binding macromolecular substrates that lend the transporter to carry its substrates to the cytoplasm in vesicles.

of ileum at each time point were prepared. The tissue sections were processed for immunohistochemical analysis using ASBT antibody (C-terminal, 1 : 100) and IBABP antibody to observe the spatial distribution of ASBT and IBABP proteins (apical to sub-apical region) from the ileum of LHe-*tetra*D-treated rats compared to untreated rats. Again, tissue samples at each time points were lysed in 1% cold RIPA buffer supplemented with protease inhibitors and phosphatase inhibitors in PBS. Protein extracts (70 μg) were separated by SDS-PAGE on 12% and 15% gels and blotted against ASBT and IBABP antibody, respectively.

1. Meier, P. J. & Stieger, B. Bile salt transporters. *Annu. Rev. Physiol.* **64**, 635–661 (2002).
2. Lazaridis, K. N. *et al.* Rat cholangiocytes absorb bile acids at their apical domain via the ileal sodium-dependent bile acid transporter. *J. Clin. Invest.* **100**, 2714–2721 (1997).
3. Claro da Silva, T., Polli, J. E. & Swaan, P. W. The solute carrier family 10 (SLC10): beyond bile acid transport. *Mol. Aspects Med.* **34**, 252–269 (2013).
4. Hu, N. J., Iwata, S., Cameron, A. D. & Drew, D. Crystal structure of a bacterial homologue of the bile acid sodium symporter ASBT. *Nature* **478**, 408–411 (2011).
5. van der Velden, L. M. *et al.* Monitoring bile acid transport in single living cells using a genetically encoded Forster resonance energy transfer sensor. *Hepatology* **57**, 740–752 (2013).
6. Gong, Y. Z., Everett, E. T., Schwartz, D. A., Norris, J. S. & Wilson, F. A. Molecular cloning, tissue distribution, and expression of a 14-kDa bile acid-binding protein from rat ileal cytosol. *Proc. Natl. Acad. Sci. U. S. A.* **91**, 4741–4745 (1994).
7. Kramer, W., Girbig, F., Gutjahr, U. & Kowalewski, S. Radiation-Inactivation Analysis of the Na+ Bile-Acid Cotransport System from Rabbit Ileum. *Biochem. J.* **306**, 241–246 (1995).
8. Rao, A. *et al.* The organic solute transporter alpha-beta, Ostalpha-Ostbeta, is essential for intestinal bile acid transport and homeostasis. *Proc. Natl. Acad. Sci. U. S. A.* **105**, 3891–3896 (2008).
9. Tamai, I. & Tsuji, A. Carrier-mediated approaches for oral drug delivery. *Adv. Drug Deliv. Rev.* **20**, 5–32 (1996).
10. Al-Hilal, T. A., Alam, F. & Byun, Y. Oral drug delivery systems using chemical conjugates or physical complexes. *Adv. Drug Deliv. Rev.* **65**, 845–864 (2013).
11. Rajendran, L., Knolker, H. J. & Simons, K. Subcellular targeting strategies for drug design and delivery. *Nat. Rev. Drug Discov.* **9**, 29–42 (2010).
12. Hurley, J. H., Boura, E., Carlson, L. A. & Rozycki, B. Membrane budding. *Cell* **143**, 875–887 (2010).
13. Bareford, L. M. & Swaan, P. W. Endocytic mechanisms for targeted drug delivery. *Adv. Drug Deliv. Rev.* **59**, 748–758 (2007).
14. Petrus, A. K., Fairchild, T. J. & Doyle, R. P. Traveling the vitamin B12 pathway: oral delivery of protein and peptide drugs. *Angew. Chem. Int. Ed. Engl.* **48**, 1022–1028 (2009).
15. He, W. *et al.* FcRn-mediated antibody transport across epithelial cells revealed by electron tomography. *Nature* **455**, 542–546 (2008).
16. Meier, Y. *et al.* Regional distribution of solute carrier mRNA expression along the human intestinal tract. *Drug Metab. Dispos.* **35**, 590–594 (2007).
17. Tamai, I. Oral drug delivery utilizing intestinal OATP transporters. *Adv. Drug Deliv. Rev.* **64**, 508–514 (2012).
18. Xia, X. *et al.* Degradation of the apical sodium-dependent bile acid transporter by the ubiquitin-proteasome pathway in cholangiocytes. *J. Biol. Chem.* **279**, 44931–44937 (2004).
19. Annaba, F. *et al.* Enteropathogenic Escherichia coli inhibits ileal sodium-dependent bile acid transporter ASBT. *Am. J. Physiol. Gastrointest. Liver Physiol.* **302**, G1216–1222 (2012).
20. Kooijman, E. E., Chupin, V., de Kruijff, B. & Burger, K. N. Modulation of membrane curvature by phosphatidic acid and lysophosphatidic acid. *Traffic* **4**, 162–174 (2003).
21. Baumgart, T., Capraro, B. R., Zhu, C. & Das, S. L. Thermodynamics and mechanics of membrane curvature generation and sensing by proteins and lipids. *Annu. Rev. Phys. Chem.* **62**, 483–506 (2011).
22. Stachowiak, J. C. *et al.* Membrane bending by protein-protein crowding. *Nat. Cell Biol.* **14**, 944–949 (2012).
23. Stachowiak, J. C., Hayden, C. C. & Sasaki, D. Y. Steric confinement of proteins on lipid membranes can drive curvature and tubulation. *Proc. Natl. Acad. Sci. U. S. A.* **107**, 7781–7786 (2010).
24. Xu, S., Olenyuk, B. Z., Okamoto, C. T. & Hamm-Alvarez, S. F. Targeting receptor-mediated endocytotic pathways with nanoparticles: rationale and advances. *Adv. Drug Deliv. Rev.* **65**, 121–138 (2013).
25. Grant, B. D. & Donaldson, J. G. Pathways and mechanisms of endocytic recycling. *Nat. Rev. Mol. Cell Biol.* **10**, 597–608 (2009).
26. Doherty, G. J. & McMahon, H. T. Mechanisms of Endocytosis. *Annu. Rev. Biochem.* **78**, 857–902 (2009).
27. Ikonen, E. Cellular cholesterol trafficking and compartmentalization. *Nat. Rev. Mol. Cell Bio.* **9**, 125–138 (2008).
28. Varkouhi, A. K., Scholte, M., Storm, G. & Haisma, H. J. Endosomal escape pathways for delivery of biologicals. *J. Control. Release* **151**, 220–228 (2011).
29. El-Sayed, A., Futaki, S. & Harashima, H. Delivery of macromolecules using arginine-rich cell-penetrating peptides: ways to overcome endosomal entrapment. *AAPS J.* **11**, 13–22 (2009).
30. Bolte, S. & Cordelieres, F. P. A guided tour into subcellular colocalization analysis in light microscopy. *J. Microsc-Oxford.* **224**, 213–232 (2006).
31. van Steensel, B. *et al.* Partial colocalization of glucocorticoid and mineralocorticoid receptors in discrete compartments in nuclei of rat hippocampus neurons. *J. Cell Sci.* **109 (Pt 4)**, 787–792 (1996).

Acknowledgments

We thank S.M. Riajul Wahab for the collaboration in molecular biology works and Ms Eun Jung Kang for the technical supports with confocal imaging. This study was supported by a grant from the World Class University (WCU) program (grant no. R31-2008-000-10103), the Converging Research Center Program (grant no. 2012K-001398) and the Bio & Medical Technology Development Program (grant no. 2012028833) through the National Research Foundation of Korea (NRF) funded by the Ministry of Education, Science and Technology, Republic of Korea and Mediplex Corp., Korea.

Author contributions

T.A.A. conceived, designed, and performed majority of the experiments including analyzing the data. S.C., F.A. and J.P. assisted with the synthesis and helped in planning the study. S.C. assisted with schematics illustrations. J.P. performed binding affinity study. K.L. performed the transmission electron microscopy experiments and H.J. supervised the work. K.K., I.K., I.K., S.K. and Y.B. discussed the results and commented on the manuscript. T.A.A. and Y.B. wrote the manuscript with assistance from I.K. and S.K. Correspondence and requests for materials should be addressed to Y.B.

Additional information

Supplementary information accompanies this paper at http://www.nature.com/scientificreports

Competing financial interests: The authors declare no competing financial interests.

How to cite this article: Al-Hilal, T.A. *et al*. Functional transformations of bile acid transporters induced by high-affinity macromolecules. *Sci. Rep.* **4**, 4163; DOI:10.1038/srep04163 (2014).

SCIENTIFIC REPORTS

Corrigendum: Functional transformations of bile acid transporters induced by high-affinity macromolecules

Taslim A. Al-Hilal, Seung Woo Chung, Farzana Alam, Jooho Park, Kyung Eun Lee, Hyesung Jeon, Kwangmeyung Kim, Ick Chan Kwon, In-San Kim, Sang Yoon Kim & Youngro Byun

Scientific Reports **4**:4163; doi: 10.1038/srep04163; published online 25 February 2014; updated on 05 August 2015

This Article contains an error in Figure 6a where the 0 h immunohistochemistry data is duplicated for 24 h. The correct Figure 6 appears below as Figure 1.

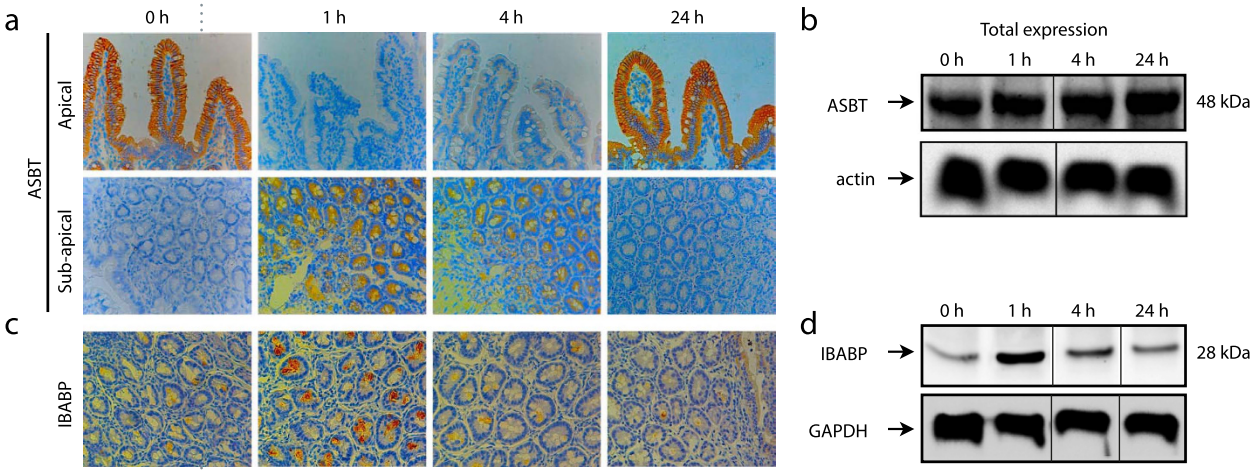

Figure 1.